XLI CILAMCE
XLI Ibero-Latin American Congress on Computational Methods in Engineering
16-19 November, 2020 FOZ DO IGUAÇU PARANÁ - BRAZIL

On interpolation methods for modeling low-density elements in topology optimization of geometrically nonlinear structures

Vinicius O. Fontes[1], André X. Leitão[1], Anderson Pereira[1]

[1]*Dept. of Mechanical Engineering, Pontifical Catholic University of Rio de Janeiro*
R. Marquês de São Vicente, 225, 22451-900, RJ/Rio de Janeiro, Brazil
vinicius.fontes@aluno.puc-rio.br, andrex.leitao@aluno.puc-rio.br, anderson@puc-rio.br

Abstract.

Modeling void regions is one of the main challenges in topology optimization of geometrically nonlinear structures due to the excessive distortions of low-density elements. Several solutions to this problem have been suggested in the literature, including interpolation methods such as the Energy Interpolation scheme and the Additive Hyperelasticity technique. These methods consist in interpolating each element's model between the original material for solid elements and a less stiff model for the low-density ones. In this work, we introduce the general framework for topology optimization that handles several hyperelastic materials. Both interpolation methods are explored in the solution of classic compliance-minimization problems under the assumption of plane strain conditions with numerical results for two benchmark topology optimization problems being provided.

Keywords: Topology optimization, Large deformations, Energy interpolation, Additive hyperelasticity, Hyperelastic material

1 Introduction

In the standard element density-based formulation of Topology Optimization (TO), a constant design variable, called density by some authors, is commonly assigned to each finite element of a discretized domain. In this context, every finite element is a potential void or solid material, such that void regions within the design domain are filled with low-density finite elements. It is known that such elements might suffer from excessive distortions when considering large deformations, which may jeopardize convergence of the Newton-Raphson (NR) method. Some authors have proposed solutions such as removing the low-density elements from the convergence criterion (Buhl et al. [1]), removal and reintroduction of low-density elements from the mesh (Bruns and Tortorelli [2]), using polyconvex models (Lahuerta et al. [3]) and super element condensation (Jie et al. [4]).

To address the numerical instabilities, two interpolation methods suggested in the literature are considered in this work. They consist of modeling low-density elements as a less stiff material: the Energy Interpolation (EI) scheme proposed by Wang et al. [5] models them according to the small deformation theory, while the Additive Hyperelasticity (AH) technique of Luo et al. [6] uses a soft incompressible Yeoh material. Chen et al. [7] incorporated the AH into ANSYS by using a nearly incompressible Yeoh model, and observed that the EI method could not be easily implemented due to its complexity.

A vast literature review on geometrically nonlinear TO can be found in the work of Leitão [19], who applied a modified interpolation scheme based on the formulations of Pajot [9] and Wang et al. [5], while also providing discussions and comparison of the proposed scheme for the St. Venant Kirchhoff (SVK) material model. Recently, relevant works such as Klarbring and Strömberg [10] have used hyperelastic models that are known to better represent a body's behavior undergoing large compressions. A Matlab program based on `PolyTop` (Talischi et al. [11]) was developed to compare the optimized designs obtained using the two interpolation methods, where some changes to the original implementations were adopted to work with different hyperelastic materials on plane strain.

The outline of this article is as follows: Section 2 introduces the main features of TO; in Section 3, material models are defined, as well as the formulations for both the EI and the AH methods; Section 4 presents the results for each of the studied techniques and in Section 5 we present our final remarks.

2 Topology Optimization

The goal of topology optimization is to find the best material distribution in a domain that minimizes a given objective function (Bendsøe and Sigmund [12]). The domain is often discretized into finite elements and a design variable x_e is assigned to each element e representing whether it exists ($x_e = 1$) or not ($x_e = 0$). Although "0 or 1" values are desired, the design variable may assume any value in between, such that the optimization problem can be defined as follows:

$$\min_{x} \quad c = \boldsymbol{f}^T \boldsymbol{u} \tag{1a}$$

$$\text{subject to} \quad \frac{1}{V}\sum_{e=1}^{N_e} V_e \bar{x}_e \leqslant V_{frac}, \tag{1b}$$

$$0 \leqslant x_e \leqslant 1, \tag{1c}$$

$$\text{with} \quad \boldsymbol{r}(\boldsymbol{x}, \boldsymbol{u}) = \boldsymbol{0}. \tag{1d}$$

Equation (1a) is the objective function, the end-compliance of the structure that is computed from the nodal external force vector $\boldsymbol{f}$ and displacement vector $\boldsymbol{u}$. The volume constraint in (1b) establishes that the strucuture's allowed volume should be less than a given fraction, V_{frac}. V is the initial volume of the domain whereas the current volume of the structure is computed from the original volume of each element V_e multiplied by its respective $\bar{x}_e$ defined in Section 2.2. The residual $\boldsymbol{r}$ is satisfied at every TO iteration and is defined as the difference between $\boldsymbol{f}$ and the internal force vector. For information on finite element implementation, the reader is referred to Kim [13]. The Method of Moving Asymptotes (MMA), introduced by Svanberg [14], is used to update the design variables.

2.1 Design Variable Filter

The linear filter proposed by Bruns and Tortorelli [15] is used in this work and consists in a weighted average of the design variables within a radius r_{min}. The filtered variable $\tilde{x}_e$ of the eth element is given by

$$\tilde{x}_e = \frac{\sum_{i=1}^{N_e} w_{e,i} x_i}{\sum_{i=1}^{N_e} w_{e,i}}, \tag{2}$$

where $w_{e,i}$ is the weight function computed from the distance $d_{e,i}$ between elements e and i as follows:

$$w_{e,i} = \max\left(1 - \frac{d_{e,i}}{r_{min}}, 0\right). \tag{3}$$

2.2 Projection and Penalization

A smoothed Heaviside projection introduced by Wang et al. [16] is applied to the filtered variable such that the projected variable $\bar{x}_e$ of the eth element is obtained from

$$\bar{x}_e(\tilde{x}_e) = \frac{\tanh(\beta\eta) + \tanh[\beta(\tilde{x}_e - \eta)]}{\tanh(\beta\eta) + \tanh[\beta(1-\eta)]}, \tag{4}$$

in which β is the sharpness parameter and η is the density threshold. For this work, $\eta = 0.5$ is fixed, but β is subject to a continuation procedure, starting at $\beta = 4$. The Solid Isotropic Material with Penalization (SIMP) method (Rozvany [17]) is applied to the projected variable, so the penalized variable $\hat{x}_e$ comes from

$$\hat{x}_e(\bar{x}_e) = (1 - \epsilon)\bar{x}_e^p + \epsilon, \tag{5}$$

where ϵ is a small value to avoid numerical problems – here, it is set to $10^{-9}E$ (or increased to $10^{-4}E$ when convergence is not achieved), for E being the Young modulus. In this work, element's density refers to $\hat{x}_e$.

3 Interpolation Methods for Hyperelastic Materials

In order to change an element's stiffness during TO, an approach inspired on Klarbring and Strömberg [10] is reproduced in this work: the element's strain energy ϕ_e is multiplied by the density of its respective element. Table 1 presents the strain energy density ϕ for the materials considered in this work as a function of the principal and reduced invariants of the Cauchy-Green strain tensor, I_i and J_i, respectively. Models 2 through 7 were introduced by Klarbring and Strömberg [10] and references therein.

Table 1. Material models used in this work.

Model	Type	Strain Energy Density (ϕ)
ϕ_1	SVK	$\frac{\lambda}{8}(I_1-3)^2+\frac{\mu}{4}(I_1^2-2I_1-2I_2+3)$
ϕ_2	Modified SVK	$\frac{\lambda}{2}(\ln J)^2+\frac{\mu}{4}(I_1^2-2I_1-2I_2+3)$
ϕ_3		$\lambda(J-\ln J-1)+\frac{\mu}{4}(I_1^2-2I_1-2I_2+3)$
ϕ_4		$\frac{\lambda}{2}(J-1)^2+\frac{\mu}{4}(I_1^2-2I_1-2I_2+3)$
ϕ_5	Modified nH	$\frac{\lambda}{2}(\ln J)^2-\mu\ln J+\frac{\mu}{2}(I_1-3)$
ϕ_6		$\lambda(J-\ln J-1)-\mu\ln J+\frac{\mu}{2}(I_1-3)$
ϕ_7		$\frac{\lambda}{2}(J-1)^2-\mu\ln J+\frac{\mu}{2}(I_1-3)$
ϕ_8	Mooney-Rivlin	$A_{10}(J_1-3)+A_{01}(J_2-3)+\frac{\kappa}{2}(J-1)^2$
ϕ_9	Yeoh	$\sum_{m=1}^{3}A_{m0}(J_1-3)^m+\sum_{n=1}^{2}\frac{1}{D_n}(J-1)^{2n}$

The constants λ and μ are the Lamé parameters and $\kappa=\lambda+2\mu/3$ is the bulk modulus, that may also be defined as a function of the Young modulus and Poisson coefficient ν. A_{mn} are hyperelastic material parameters, D_i are the compressibility parameters, J is the Jacobian and J_i are the reduced invariants. The strain energy density ϕ_{NL} of a given nonlinear model in Table 1, is used to calculate ϕ_e according to the interpolation as

$$\phi_e=\begin{cases}\hat{x}_e\phi_{NL}(\boldsymbol{u}_e) & \text{for no interpolation,}\\ [\phi_{NL}(\gamma_e\boldsymbol{u}_e)-\phi_L(\gamma_e\boldsymbol{u}_e)+\phi_L(\boldsymbol{u}_e)]\,\hat{x}_e & \text{for EI,}\\ \hat{x}_e\phi_{NL}(\boldsymbol{u}_e)+(1-\hat{x}_e)\phi_Y(\boldsymbol{u}_e) & \text{for AH,}\end{cases} \tag{6}$$

where ϕ_L and ϕ_Y are the strain energy density under small deformation and for a soft Yeoh model (ϕ_9), respectively. The parameters for ϕ_Y used in this work are presented in Table 2 alongside Chen et al. [7], who also considered the nearly-incompressible additive Yeoh model in the AH method.

Table 2. Material parameters for nearly incompressible Yeoh model, ϕ_Y.

Author	Formulation	A_{10}	A_{20}	D_1	D_2
Chen et al. [7]	Plane stress	$10^{-9}E$	Variable	10^{-9}	10^{6}
This work	Plane strain	$10^{-9}E$	$10^{-9}E$	10^{9}	10^{9}

The interpolation parameter γ_e is such that when $\gamma_e=1$ the element is modeled by the nonlinear formulation and for $\gamma_e=0$ it behaves according to the small deformation theory, as follows:

$$\gamma_e(\bar{x}_e)=\frac{\tanh(\beta_1\rho_0)+\tanh[\beta_1(\bar{x}_e^p-\rho_0)]}{\tanh(\beta_1\rho_0)+\tanh[\beta_1(1-\rho_0)]}, \tag{7}$$

where $\beta_1 = 500$ and $\rho_0 = 0.01$.

To better illustrate the interpolation methods' effects, a C-shaped structure subject to the loads indicated in Fig. 1a is analyzed with ϕ_1 for $E = 1$ Pa and $\nu = 0.3$ ($\lambda = 0.5769$ Pa, $\mu = 0.3846$ Pa and $\kappa = 0.8333$ Pa). The mesh is composed by 10×10 4-node quadrilateral elements on plane strain, with the void region being composed of 9×9 elements with stiffness $10^{-9}E$. Different interpolation methods may converge to the same deformed structure, which can be seen by comparing the results with the case without the void region depicted in Fig. 1b.

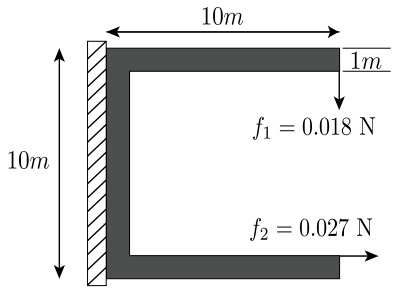

(a) Problem's domain (adapted from Wang et al. [5]).

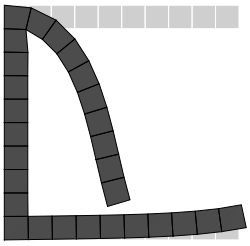

(b) Deformed structure without void regions.

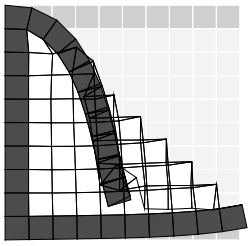

(c) Deformed structure without interpolation.

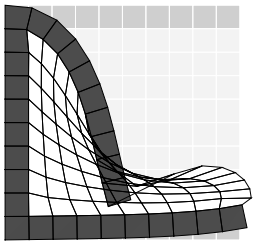

(d) Deformed structure using the EI method.

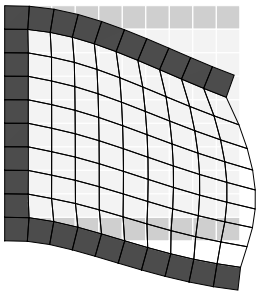

(e) Deformed structure using the AH method ($D_1 = 2/\kappa = 2.4$ Pa).

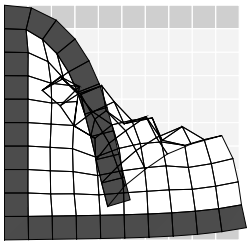

(f) Deformed structure using the AH method ($D_1 = 10^9$).

Figure 1. C-Shape problem and results with different interpolation models for plane strain state. Undeformed mesh is represented in lighter shades of gray.

The AH method in particular is very sensitive to the compressibility parameters D_i for the additive material ϕ_Y: Fig. 1e presents a stiff response when D_1 is set to the usual value suggested in commercial programs, *e.g.* Abaqus Dassault [18, Section 4.6.1]. Thus, a smaller value is required to achieve the desired result (see Fig. 1f). The proper choice of material parameters depends on the formulation, as shown in Table 2.

4 Results

Two benchmark problems with unitary thickness, *c.f.* Fig. 2, are used to gauge the performance of the interpolation methods considered in this work, where $E = 3$ GPa and $\nu = 0.4$ ($\lambda = 4.286$ GPa, $\mu = 1.071$ GPa and $\kappa = 5.000$ GPa). The value of V_{frac} is 0.5 for the cantilever beam problem and 0.1 for the clamped beam problem. The design variables are set to unity at the start of the optimization and their change is limited at $p = 3$ by scaling the increment $\Delta\boldsymbol{x}$ so its maximum component is $\Delta x_{lim} = 0.1$.

The mesh is composed by 120 x 30 elements for the cantilever beam and by 120 x 40 elements for the clamped beam problem, with 4-node quadrilaterals used in both cases. The external load in Fig. 2b is distributed over 2×2 elements, represented by the black square. Notice that all analysis were conducted under the plane strain condition, as opposed to plane stress in the works of Luo et al. [6] and Chen et al. [7]. The finite element analysis considered a constant load step $\Delta P = 0.1P$, reduced to $0.01P$ when the criterion was not met in 20 NR iterations. The displacement criterion was met when $\|\boldsymbol{u}\|_2 < 10^{-3}$. The following continuation scheme is used to smoothly steer the solution to an optimum, while achieving a "0 and 1" pattern by increasing β at the end of the process:

- For $1 \leq p < 2$: p is updated every 2 iterations;
- For $2 \leq p < 3$: p is updated every 5 iterations;
- For $p = 3$: p is not updated anymore. β is doubled every 10 iterations up to 64.

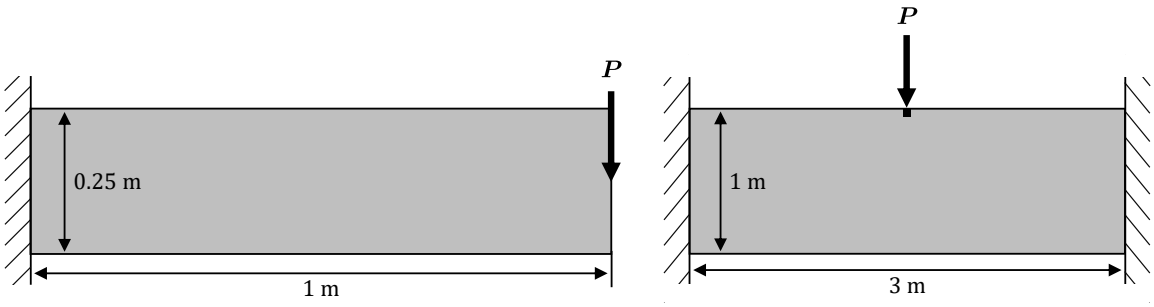

(a) Cantilever beam. (b) Clamped Beam.

Figure 2. Benchmark problems.

The cantilever problem was solved for $P = 144$ kN even without using interpolations, as indicated in Fig. 3. This is due to the elements' deformations, which are not large enough to cause numerical instabilities, yielding results similar to Buhl et al. [1] and Lahuerta et al. [3].

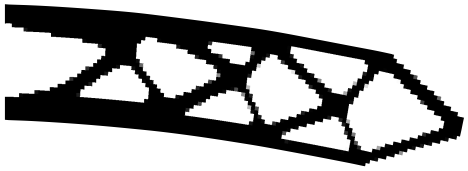

(a) No interpolation ($c = 20.8750$ kJ).

(b) Energy interpolation ($c = 20.9029$ kJ). (c) Additive hyperelasticity ($c = 20.8750$ kJ).

Figure 3. Deformed optimized cantilever beam for $P = 144$ kN with SVK model.

We were able to achieve convergence for higher loads and nonlinear models (presented in Table 1) only with the EI scheme. Nevertheless, the results were similar to those found with the linear SVK model in previous works – such as Leitão [19]. Some cases showed convergence issues and required extra techniques, as indicated in Fig. 4.

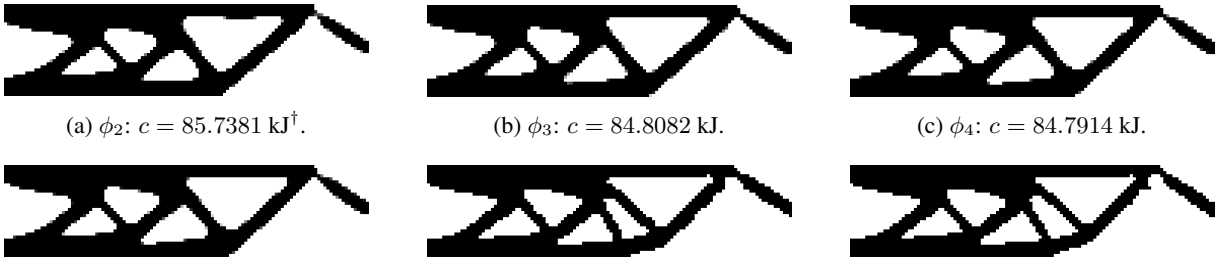

(a) ϕ_2: $c = 85.7381$ kJ†. (b) ϕ_3: $c = 84.8082$ kJ. (c) ϕ_4: $c = 84.7914$ kJ.

(d) ϕ_5: $c = 84.8863$ kJ‡. (e) ϕ_6: $c = 85.6145$ kJ†‡. (f) ϕ_7: $c = 86.5738$ kJ†.

Figure 4. Optimized cantilever beam using modified SVK (top row) and nH (bottom row).
†: Results for $\beta = 32$; ‡: Δx_{lim} set to 0.2 at $p = 2.5$ and step size reduced to $0.5\%P$.

The original work by Wang et al. [5] proposed the penalization of the element's Young modulus, which limited the choice of models that could be implemented. By penalizing the strain energy instead (see eq. (6)), any

hyperelastic model may be used, such as Mooney-Rivlin and Yeoh. These models were optimized for $P = 300$ kN and constants $A_{mn} = \mu/2$ and $D_1 = D_2 = \kappa/2$. This choice of A_{mn} makes it so the Mooney-Rivlin model is twice as stiff than Yeoh's, causing the difference shown in Fig. 5.

(a) ϕ_8: Mooney-Rivlin model ($c = 52.1916$ kJ). (b) ϕ_9: Yeoh model ($c = 85.1235$ kJ).

Figure 5. Cantilever beam optimized using other hyperelastic materials.

The clamped beam problem was solved for a load $P = 230$ kN with the EI method, as depicted in Fig. 6, where the topology has been optimized to resist the buckling effect that occurs when the applied force is too high. The other methods did not converge for this load level because the convergence criterion was not met within 1000 NR iterations per load step, even when the load step was reduced to $0.01P$.

Figure 6. Optimized topology for the clamped beam using the EI method for $P = 230$ kN ($c = 11.5027$ kJ).

5 Conclusions

In this article, we have presented a general topology optimization framework in development considering finite deformations that is capable of handling different hyperelastic materials. The proposed framework was able to implement two interpolation methods: the Energy Interpolation (EI) scheme proposed by Wang et al. [5], and the Additive Hyperelasticity (AH) of Luo et al. [6]. Two benchmark examples were presented to showcase the effectiveness of different types of material models and interpolation methods. In the first example, we considered a cantilever beam design with nine different hyperelastic models. The results indicated that, in most cases, the final design was not significantly influenced by the choice of material; the same conclusion drawn by Wang et al. [5]. In the second example, we considered the classical double clamped beam design that we were only able to optimize with the EI scheme, since the other methods did not converge within the established parameters.

The use of nearly incompressible materials to model the low-density elements has shown to be less efficient than the small-deformation theory on plane strain, as illustrated in Fig. 1f. This happens due to the fact that highly incompressible low-density elements are not able to deform in the out-of-plane direction when under compression on plane strain. Therefore, adjusting the materials parameters is paramount to achieve convergence, otherwise an undesirable response can be obtained, as shown in Fig. 1e. However, since this work did not consider the update scheme on the additive Yeoh model's parameters proposed by Luo et al. [6], the optimization process with the AH method was jeopardized. A proper adaptation of this update scheme to plane strain problems is likely to present better results.

Both interpolation methods require the computation of an extra stiffness matrix and internal force vector per element. However, for the EI method, these matrices are linear and constant, so they can be computed only once for each TO problem, while the extra matrices required for the AH method are nonlinear and should be recalculated at every NR iteration. Therefore, for large scale problems, the AH method may be more computationally costly.

Lastly, the use of a smoothed Heaviside projection in eq. (4) can modify an element's density too abruptly for high values of β. This may lead to undesirable roughness in the final topology, as seen in Fig. 4, where the β parameter had to be reduced in some cases. Further investigation on the behavior of projection function and how it affects the optimization process can be carried out in future studies. One way to circumvent this issue and achieve near black-and-white designs is by removing the filter effect at the last optimization stage (when $p = 3$) as done by Leitão [19] with satisfactory results. We also emphasize that an optimal set of techniques and parameters to handle geometrically nonlinear TO is yet to be found.

Acknowledgements. The authors would like to express their gratitude for the financial support provided by CAPES (Coordination for the Improvement of Higher Education Personnel) and CNPq (National Council for Scientific and Technological Development). The authors also appreciate the help from professor Krister Svanberg for sharing the MMA code in Matlab.

Authorship statement. The authors hereby confirm that they are the sole liable persons responsible for the authorship of this work, and that all material that has been herein included as part of the present paper is either the property (and authorship) of the authors, or has the permission of the owners to be included here.

References

[1] Buhl, T., Pedersen, C. B., & Sigmund, O., 2000. Stiffness design of geometrically nonlinear structures using topology optimization. *Structural and Multidisciplinary Optimization*, vol. 19, n. 2, pp. 93–104.
[2] Bruns, T. E. & Tortorelli, D. A., 2003. An element removal and reintroduction strategy for the topology optimization of structures and compliant mechanisms. *International journal for numerical methods in engineering*, vol. 57, n. 10, pp. 1413–1430.
[3] Lahuerta, R. D., Simões, E. T., Campello, E. M., Pimenta, P. M., & Silva, E. C., 2013. Towards the stabilization of the low density elements in topology optimization with large deformation. *Computational Mechanics*, vol. 52, n. 4, pp. 779–797.
[4] Jie, H., Xiaojun, G., Jihong, Z., Jie, W., & Zhang, W., 2020. Topology optimization of joint load control with geometrical nonlinearity. *Chinese Journal of Aeronautics*, vol. 33, n. 1, pp. 372–382.
[5] Wang, F., Lazarov, B. S., Sigmund, O., & Jensen, J. S., 2014. Interpolation scheme for fictitious domain techniques and topology optimization of finite strain elastic problems. *Computer Methods in Applied Mechanics and Engineering*, vol. 276, pp. 453–472.
[6] Luo, Y., Wang, M. Y., & Kang, Z., 2015. Topology optimization of geometrically nonlinear structures based on an additive hyperelasticity technique. *Computer methods in applied mechanics and engineering*, vol. 286, pp. 422–441.
[7] Chen, Q., Zhang, X., & Zhu, B., 2019. A 213-line topology optimization code for geometrically nonlinear structures. *Structural and Multidisciplinary Optimization*, vol. 59, n. 5, pp. 1863–1879.
[19] Leitão, A. X., 2019. Topology optimization of geometrically nonlinear structures considering an energy interpolation scheme. Master's thesis, Department of Mechanical Engineering, Pontifical Catholic University of Rio de Janeiro, Rio de Janeiro, Brazil.
[9] Pajot, J. M., 2006. Topology optimization of geometrically nonlinear structures including thermo-mechanical coupling. Ph.d. thesis, Department of Aerospace Engineering Science, University of Colorado at Boulder, Boulder, USA.
[10] Klarbring, A. & Strömberg, N., 2013. Topology optimization of hyperelastic bodies including non-zero prescribed displacements. *Structural and Multidisciplinary Optimization*, vol. 47, n. 1, pp. 37–48.
[11] Talischi, C., Paulino, G. H., Pereira, A., & Menezes, I. F., 2012. PolyTop: a matlab implementation of a general topology optimization framework using unstructured polygonal finite element meshes. *Structural and Multidisciplinary Optimization*, vol. 45, n. 3, pp. 329–357.
[12] Bendsøe, M. P. & Sigmund, O., 2013. *Topology optimization: theory, methods, and applications*. Springer Science & Business Media.
[13] Kim, N.-H., 2014. *Introduction to nonlinear finite element analysis*. Springer Science & Business Media.
[14] Svanberg, K., 1987. The method of moving asymptotes - a new method for structural optimization. *International journal for numerical methods in engineering*, vol. 24, n. 2, pp. 359–373.
[15] Bruns, T. E. & Tortorelli, D. A., 2001. Topology optimization of non-linear elastic structures and compliant mechanisms. *Computer methods in applied mechanics and engineering*, vol. 190, n. 26-27, pp. 3443–3459.
[16] Wang, F., Lazarov, B. S., & Sigmund, O., 2011. On projection methods, convergence and robust formulations in topology optimization. *Structural and Multidisciplinary Optimization*, vol. 43, n. 6, pp. 767–784.
[17] Rozvany, G. I. N., 2001. On design-dependent constraints and singular topologies. *Structural and Multidisciplinary Optimization*, vol. 21, n. 2, pp. 164–172.
[18] Dassault, S., 2007. Abaqus analysis user's manual. *Simulia Corp. Providence, RI, USA*.